

Original Research

# Assessment of the *in Vitro* Effects of Folate Core–Shell Conjugated Iron Oxide Nanoparticles as a Potential Agent for Acute Leukemia Treatment

Ghada M. Nasr<sup>1</sup>, Osama M. Thawabieh<sup>1,\*</sup>, Randa M. Talaat<sup>1</sup>, Mahmoud Moawad<sup>2</sup>,  
Manal O. El Hamshary<sup>1</sup><sup>1</sup>Department of Molecular Diagnostics and Therapeutics, Genetic Engineering & Biotechnology Research Institute, University of Sadat City, 32958 Sadat, Egypt<sup>2</sup>Pathology Department, National Cancer Institute, Cairo University, 11796 Giza, Egypt\*Correspondence: [os\\_thawabi@yahoo.com](mailto:os_thawabi@yahoo.com) (Osama M. Thawabieh)

Academic Editor: Peter Brenneisen

Submitted: 25 June 2023 Revised: 18 August 2023 Accepted: 26 September 2023 Published: 23 April 2024

## Abstract

**Background and Objective:** There is a growing need to comprehend the potential outcomes of nanoparticles (NPs) on human well-being, including their potential for detecting and treating leukemia. This study examined the role of iron folate core–shell and iron oxide nanoparticles in inducing apoptosis and altering the expression of the B-cell lymphoma 2 (*Bcl-2*), Bcl-2 associated X-protein (*Bax*), and *Caspase-3* genes in leukemia cells. **Methods:** The obtained iron oxide and iron folate core–shell nanoparticles were analyzed using a variety of analytical techniques, including ultraviolet-visible (UV-Vis) absorption spectroscopy, Fourier transform infrared spectroscopy (FTIR), X-ray diffraction (XRD), dynamic light scattering (DLS), zeta potential, and transmission electron microscopy (TEM). Additionally, FTIR and UV-Vis were used to characterize doxorubicin. The MTT test was utilized to investigate the cytotoxicity of iron oxide and iron folate core–shell nanoparticles. The expression of the apoptotic signaling proteins Bcl-2, Bax, and Caspase-3 was evaluated using the real-time reverse transcription polymerase chain reaction (RT-qPCR) method. Additionally, flow cytometry was performed to gauge the degrees of necrosis and apoptosis. **Results:** UV-Visible spectroscopy analysis showed that the generated iron oxide and iron folate core–shell NPs had a distinctive absorption curve in the 250–300 nm wavelength range. The XRD peaks were also discovered to index the spherical form with a size of less than 50 nm, which validated the crystal structure. The FTIR analysis determined the bonds and functional groups at wavenumbers between 400 and 4000  $\text{cm}^{-1}$ . A viable leukemia treatment approach is a nanocomposite consisting of iron and an iron folate core-shell necessary for inhibiting and activating cancer cell death. The nearly resistant apoptosis in the CCRF-CEM cells may have resulted from upregulating *Bax* and *Caspase-3* while downregulating *Bcl-2* expression. **Conclusions:** Our study documents the successful synthesization and characterization of iron oxide, which has excellent anticancer activities. A metal oxide conjugation with the nanoparticles' core–shell enhanced the effect against acute leukemia.

**Keywords:** leukemia; iron oxide; iron folate core–shell; apoptosis; Bcl-2; Bax; Caspase-3

## 1. Introduction

Leukemia is a type of hematological cancer characterized by complex genetic and biological features that promote invasiveness [1,2]. Leukemia's high prevalence and low survival rates are a cause of concern for researchers [3]. Leukemia can be treated using various methods, such as radiotherapy, chemotherapy, targeted therapy, immunotherapy, and stem cell transplantation [4,5]. Doxorubicin (DOX) is a well-known Food and Drug Administration (FDA)-approved anticancer drug. However, despite being an effective anti-tumor medication, DOX can cause serious side effects such as rapid excretion, short retention time, and, most notably, cardiotoxicity that can lead to life-threatening cardiomyopathy and congestive heart failure [6]. Despite researchers' efforts to improve leukemia treatment strategies, favorable outcomes have not been achieved.

In healthcare, nanotechnology is widely used for tissue healing, diagnosis, and treatment [7,8]. Among all the NPs, metal NPs have drawn particular attention because of their ability to function as various agents. Abdoli *et al.* [9] and Xu *et al.* [10] reported that metal NPs based on gold, silver, iron, and/or iron oxide have been used as cancer treatments. Iron oxide ( $\text{Fe}_3\text{O}_4$ ) nanoparticles (IONPs), a type of metal nanoparticle, have been used extensively in biomedical applications because of their unique properties [11]. According to Gonzalez-Rodriguez *et al.* [12] and Cabana *et al.* [13], IONPs are used in various biomedical applications, such as magnetic resonance imaging (MRI), contrast agents, and drug delivery in cancer therapy. According to Alphanéry [14], IONPs have been increasingly employed in hematological tumors in the past several years due to their characteristics.

Folic acid is a popular targeted ligand, particularly in cancer treatment. It is a synthetic version of vitamin B9



or folate. However, folic acid does not occur in nature; it should be noted that both names, folic acid, and folate, are frequently used interchangeably [15]. As it takes part in nucleotide synthesis, amino acid metabolism, and phospholipid production, this essential chemical is required for DNA replication and repair, RNA synthesis, and other biological processes [16]. Folate conjugation consequently offers a substrate for medication delivery that targets Folate receptor (FR). Small compounds, macromolecules, and nanocarriers have been successfully studied using this technique [17,18]. For instance, a folate-targeted nanosystem focusing on FR expression may improve leukemia treatment's capacity to target specific cells [19]. Research on the potential cytotoxicity of the folate core-shell, used as the outermost shell of magnetite iron oxide nanoparticles, has yet to be done.

The current study aimed to determine whether the doxorubicin chemotherapeutic drug, magnetite iron oxide nanoparticles, and folate core-shell conjugated with iron oxide nanoparticles was cytotoxic to human acute leukemia cell lines and a control cell line. Analysis of the treated group's *Bax*, *Bcl2*, and *Caspase-3* gene expression was performed using real-time reverse transcription polymerase chain reaction (RT-qPCR), and apoptosis was analyzed with flow cytometry.

## 2. Materials and Methods

### 2.1 Synthesis of Iron Oxide Magnetic Nanoparticles

Iron oxide nanoparticle synthesis was completed as previously described [20]. In a mixture, ferric and ferrous ions were combined at room temperature in a 1:2 molar ratio. Once the pH of the solution reached 10, 1.5 M NaOH was gradually added to the reaction to carry out the coprecipitation. The precipitate was magnetically separated and then washed with distilled water numerous times until the pH reached 7. The cleaned nanoparticles were allowed to air dry at room temperature before being used in further research.

### 2.2 Synthesis of Magnetic Iron Folate Core-Shell Nanostructure

A total of 0.1 g folic acid was added to 100 mL of deionized water, agitated for 30 minutes at 60 °C, and then exposed to ultra-sonication for two hours at 0.9 cycles and 90% amplitude. After adding 50 mL of previously prepared folic acid, 0.1 g of magnetite nanoparticles were added to 50 mL of doubled deionized water and stirred for 0.5 hours with a mechanical stirrer. The mixture was then sonicated for 6 hours (0.6 cycles and 50% amplitude).

### 2.3 Nanoparticle Characterization

#### 2.3.1 UV-Vis Absorption Spectroscopy

This study characterized the optical absorption characteristics of materials using ultraviolet-visible (UV-Vis) spectroscopy. All absorbance measurements and data ma-

nipulation were performed on a computer running Shimadzu UV probe software, and a UV/Vis spectrophotometer from the Shimadzu UV 2450 PC series (Tokyo, Japan) was used to capture the spectra. The spectrophotometer was equipped with two matching 1 cm quartz cells and had the following spectral settings: one quick scan mode and a slit width of 2 nm. The development of iron oxide nanoparticles, iron folate core-shell nanoparticles, and doxorubicin was monitored using UV-Vis spectra [21].

#### 2.3.2 The Transmutation Electron Microscope (TEM)

The size and shape of iron oxide and iron folate core-shell nanoparticles were determined using the transmission electronic microscope (TEM). The microscope (JEOL -Tokyo -Japan- JEM.1400 electron microscope) was used for the TEM characterization of nanoparticles. A drop of the nanoparticle solution was placed on a carbon grid and let dry in a desiccator before being spotted with TEM.

#### 2.3.3 FTIR Analysis

Using spectroscopic-grade potassium bromide (KBr) that was dried at 100 °C and chilled in a vacuum desiccator to minimize moisture absorption, functional groups on compounds were analyzed using FTIR (FT/IR-4X, Jasco, Japan) in the intermediate wavenumber (450–4000  $\text{cm}^{-1}$ ) for iron oxide and iron folate core-shell nanoparticles, and doxorubicin.

#### 2.3.4 Dynamic Light Scattering (DLS)

The size and size distribution of NPs were measured using the dynamic light scattering (DLS) method with the Zetasizer Nano ZS (Malvern Pananalytical Ltd, Malvern, UK). The sample was put within a cuvette made of quartz. Following equipment calibration, each sample was subjected to three measurements. Size distribution was calculated using the collected data for iron oxide and iron folate core-shell nanoparticles.

#### 2.3.5 X-Ray Diffraction (XRD)

Utilizing a Philips1820 advance diffractometer with Ni-filtered  $\text{Cu K}\alpha$  radiation and a scan rate of 0.24 per minute, powder X-ray diffraction (XRD) experiments were conducted for iron oxide and iron folate core-shell nanoparticles. Copper potassium alpha radiation (40 mA) was utilized while the device was run at a 45 kV voltage.

#### 2.3.6 Zeta Potential (ZP) Measurement

The laser Doppler electrophoresis technique was employed to quantify the particle electrostatic charge, and the findings are represented as zeta potential using the Zetasizer-nano instrument (Malvern, UK). A total of 100  $\mu\text{L}$  of the particle solution was diluted with 1.5 mL of water and added into a cuvette to determine the particle electrostatic charge (ZP) of iron oxide and iron folate core-shell nanoparticles.

**Table 1. Specific primer sequences used for real-time polymerase chain reaction (PCR).**

| Primer name    | Forward (5'-3')           | Reverse (5'-3')             |
|----------------|---------------------------|-----------------------------|
| $\beta$ -actin | CTGTCTGGCGCACCACCAT       | GCAACTAAGTCATAGTCCGC        |
| Bax            | AAGCTGAGCGAGTGTCTCAAGCGC  | TCCCGCCACAAAGATGGTCAAG      |
| Bcl-2          | AGATGTCCAGCCAGCTGCACCTGAC | AGATAGGCACCCAGGGTGATGCAAGCT |
| Caspase-3      | TTGATGCGTGATGTTTCTA       | CAATGCCACAGTCCAGTTC         |

Bcl-2, B-cell lymphoma 2; Bax, Bcl-2 associated X-protein.

#### 2.4 Anti-Tumor Activity against Different Human Cell Lines

The American Type Culture Collection (ATCC) was used to obtain the human acute lymphocytic leukemia (ALL) cell lines (CCRF-CEM, RS4; 11<sup>TM</sup>), human acute myelogenous leukemia (AML) (THP1 (TIB-202<sup>TM</sup>), Kasumi-1 (CRL-2724<sup>TM</sup>), and normal cell line (CRL-1980<sup>TM</sup>) (ATCC, Gaithersburg, MD, USA). The acute leukemia cells were typically grown in a DMEM medium. We added 2 mM of L-glutamine to the media, 100 units of penicillin G sodium, 250 ng of amphotericin B, 100 units of streptomycin sulfate, and 10% fetal bovine serum (FBS). At sub-confluence, cells were kept at 37 degrees Celsius in humidified air containing 5% carbon dioxide. At 75% confluence, cells were collected using trypsin/EDTA. Gibco®/Invitrogen, USA, was the source of all cell culture supplies. Unless otherwise specified, all compounds were purchased from Sigma-Aldrich in the United States.

As performed by ATCC, short-tandem repeat STR profiling uses multiplex PCR to simultaneously amplify the amelogenin gene and seventeen polymorphic markers, including the most informative polymorphic markers in the human genome. ATCC uses the Promega PowerPlex 18D system and the ThermoFisher Scientific GeneMapper ID-X v1.2 software to analyze the amplicons.

The Mycoplasma test was performed in all cell lines using Hoechst 33258 (Sigma-Aldrich), as recommended by ATCC (Fluorescent Hoechst staining at 500X magnification). Authentication of cell lines was performed by the authors. Mycoplasma testing was performed using the Look-out one-step Mycoplasma PCR detection kit (MP0050, Sigma-Aldrich).

#### 2.5 Cytotoxicity Assay

The cytotoxic effect of IONPs, iron folate core-shell NPs, and Doxorubicin against acute leukemia cells and CRL-1980 was estimated by MTT (3-[4,5-Dimethylthiazol]-2,5-Diphenyltetrazolium bromide) assay. During the metabolic activity, mitochondrial dehydrogenases convert the yellow tetrazolium salt of MTT to generate insoluble purple formazan crystals, which may be dissolved with detergent (acidic isopropanol). Before subjecting them to an MTT experiment, cells (5104 cells/well) were treated with a serial concentration of nanoparticles and doxorubicin (12.5, 25, 50, and 100 g/mL) at 37 °C in an FBS-free mixture for 24 hours. A 570 nm absorbance

reading was taken (FLUOstar OPTIMA; BMG Labtech GmbH, Offenburg, Germany). The percentage of MTT transformed into the insoluble formazan salt represented the relative cell viability. Information was reported as the average percentage of still-alive cells in each treatment group vs. the corresponding solvent-treated control groups. The dose-response line equation determined each chemical's half-maximal growth inhibitory concentration (IC<sub>50</sub> values).

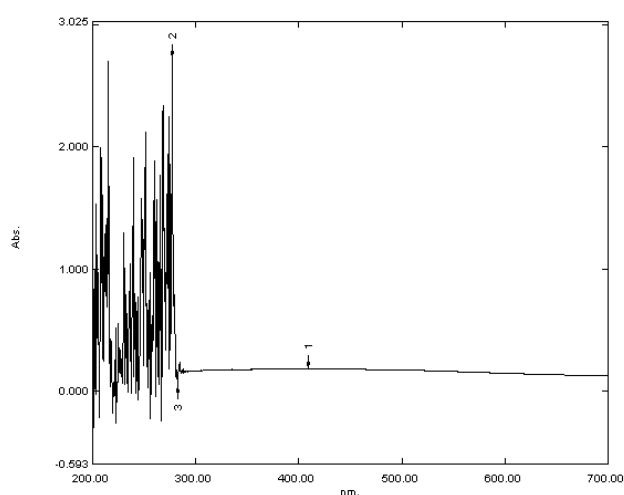


**Fig. 1. Ultraviolet-visible (UV-Vis) spectroscopy analysis of iron oxide (Fe<sub>3</sub>O<sub>4</sub>) nanoparticles (IONPs).**

#### 2.6 Quantitative Evaluation of Bcl-2, Bax, and Caspase-3 mRNA Expression Levels

Following the manufacturer's instructions, total RNA was isolated from the cell lines using the Qiagen RNA extraction kit (Qiagen Inc., Valencia, CA, USA). The Q5000 137 nanodrop (Quawell Technology, Inc., San Jose, CA, USA) was used to measure the purity and amount of RNA. The complementary DNA (cDNA) was produced by reverse transcription using a kit from Qiagen in Valencia, California, USA (Cat. No. 218161). The total reaction volume contained 100 ng of total RNA and was 20  $\mu$ L. The reference housekeeping gene used in the qPCR for apoptotic genes (*Bax*, *Bcl2*, *Caspase-3*) was actin. Thermo Scientific's Maxima SYBR Green/ROXqPCR Master Mix and specific primers were created (Table 1). The following con-

ditions were used to carry out the qPCR: initial denaturation at 95 °C for 5 min, followed by 40 cycles of denaturation at 95 °C for 15 seconds, 64 °C for 40 seconds, and strand extension at 72 °C for 1 min. Target gene critical threshold (Ct) values were standardized using the equation  $x = 2^{-\Delta\Delta C_t}$ , where  $x$  = fold change relative to control.

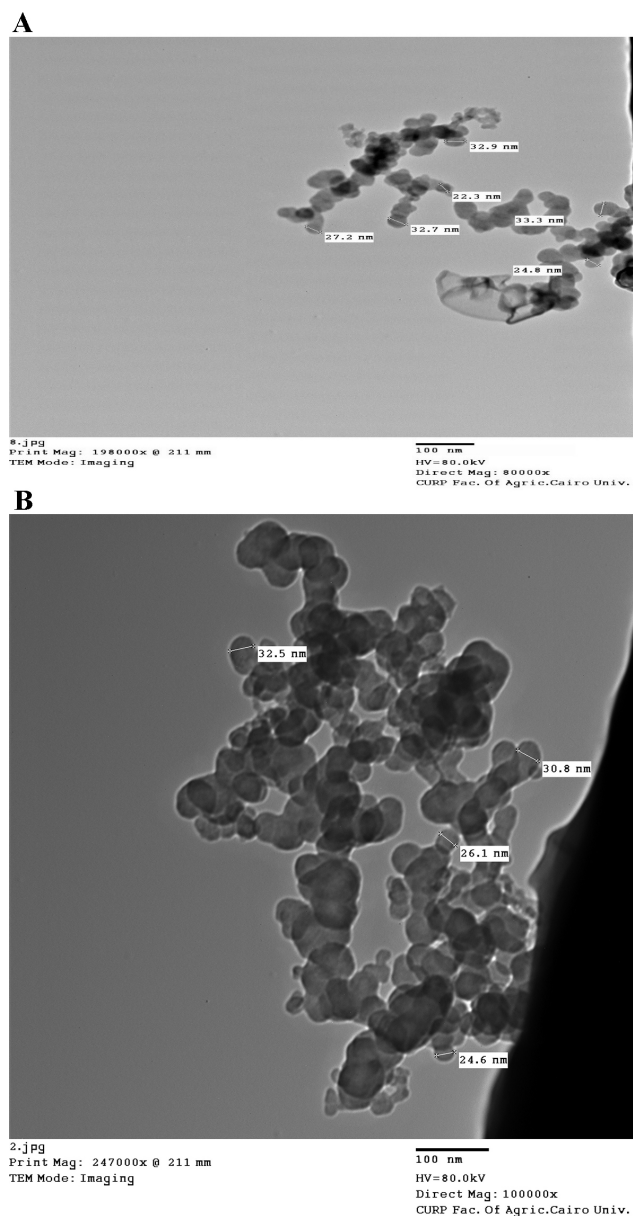


**Fig. 2.** Transmission electron microscopy (TEM) images of (A) iron oxide and (B) iron folate core-shell nanoparticles. The size of nanoparticles depends mainly on the concentration of precursor used in the synthesis of hematite, which proved that the particle size increased with the raise of the precursor concentration ( $\text{FeCl}_3 \cdot 6\text{H}_2\text{O}$ ) because the reactant with the higher concentration enhanced the merge of crystal nucleus and agglomeration of particles. Both nanoparticles prepared in favored size (7–42) nm for application purpose.

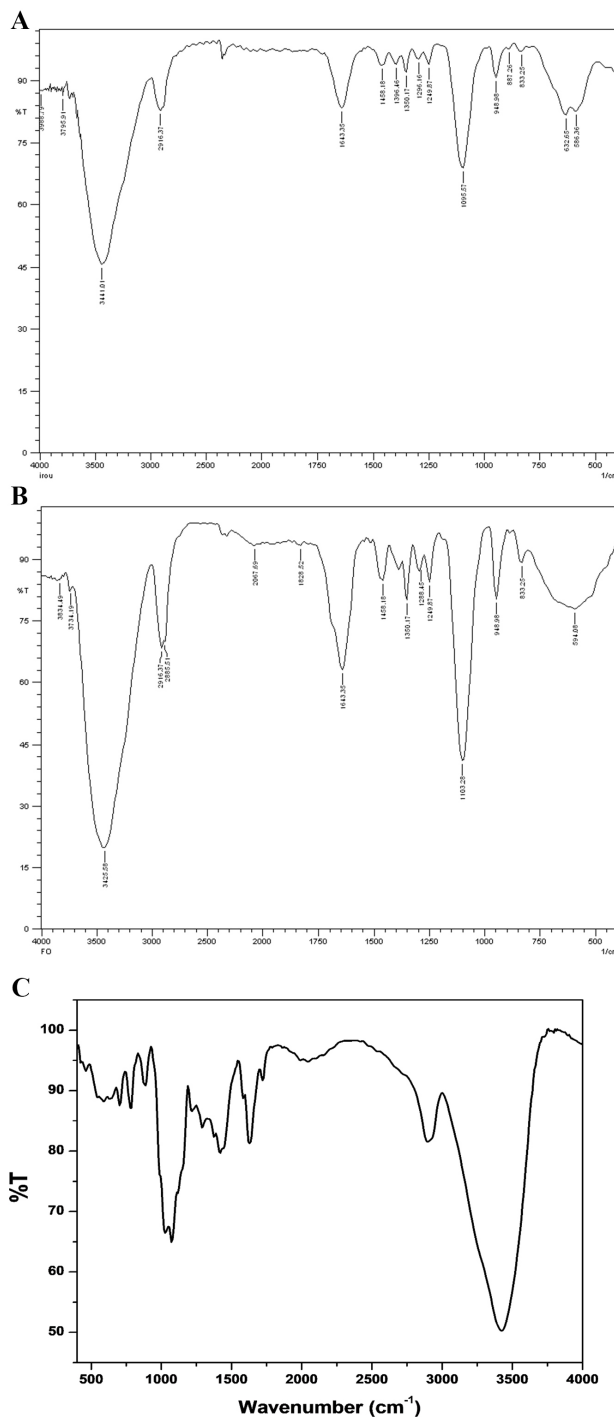


**Fig. 3.** Fourier transform infrared spectroscopy (FTIR) spectra of (A) iron oxide, (B) iron folate core-shell, and (C) doxorubicin, respectively.

### 2.7 The Flowcytometric Cell Cycle Analysis

The impact of iron oxide and iron folate core-shell nanoparticles at 100  $\mu\text{g}/\text{mL}$  on cell cycle arrest was compared to the control samples. Cell cycle distribution was analyzed using the DNA PREP Kit from Beckman Coulter USA, Inc. (Beckman Coulter 250 S. Kraemer Blvd.

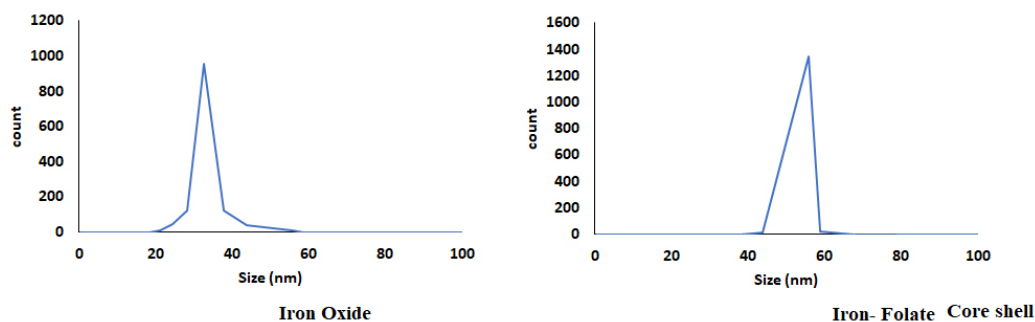


Fig. 4. The dynamic light scattering (DLS) analysis on the nanoparticle size.

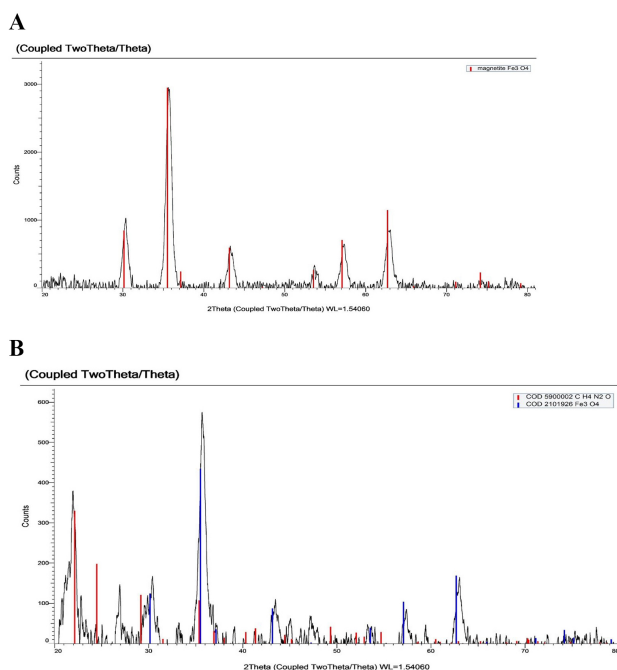


Fig. 5. X-ray diffraction (XRD) pattern of (A) iron oxide and (B) iron folate core-shell depict the diffraction of X-rays by a crystal lattice.

Brea, CA, USA). Monolayer cells from the CCRF-CEM and THP1 cell lines were treated with the  $IC_{50}$  concentration of curcumin for 5 minutes. The cell concentration was adjusted to  $3-5 \times 10^6$  cells/mL by mixing 100  $\mu$ L of single-cell suspension with 100  $\mu$ L of LPR. Finally, 2 mL of DNA PREP Stain was added, and Beckman Coulter Epics XL was used to incubate the mixture for 30 minutes.

### 2.8 Statistical Analysis

All data have been computed as mean and standard deviation (SD). One-way variance analysis (ANOVA) was utilized to compare the data with the control group.  $p < 0.05$  was shown to be significant. The Statistical Program for Social Science (SPSS) Version 28 for Windows was used for all statistical analyses (SPSS Inc., Chicago, IL, USA).

## 3. Results

### 3.1 Characterization of Nanoparticles

#### 3.1.1 UV-Vis Absorption Spectroscopy

The UV-Vis analysis confirmed the preparation of iron oxide, iron folate core-shell nanoparticles, and doxorubicin. The absorption spectra dispersed in deionized water displayed broad absorption peak at about 250–300 nm. The mean absorption for doxorubicin, iron oxide, and iron folate core-shell was  $0.262 \pm 0.381$ ,  $0.166 \pm 0.431$ , and  $0.134 \pm 0.431$ , respectively. The UV-Vis analysis of IONPs is represented in Fig. 1.

#### 3.1.2 The Transmission Electron Microscope (TEM)

According to the size distribution, the spherical micelles observed in the TEM image (Fig. 2) were nanocapsules with sizes between 7 and 42 nm.

#### 3.1.3 Fourier Transform Infrared Spectroscopy (FTIR)

The FTIR spectra of iron oxide and iron folate core-shell nanoparticles and doxorubicin are shown in Fig. 3. Peaks and troughs in the spectra indicate absorption and transmission of infrared light, revealing details about functional groups, chemical bonds, and molecular structures. Interpretation involves correlating peaks with known vibrational modes of specific functional groups.

#### 3.1.4 Dynamic Light Scattering (DLS)

The DLS analysis confirmed the size of magnitude of Iron oxide and folic core-shell nanoparticles (Fig. 4). The size of the iron oxide was 33 nm, and the iron folate core-shell was 55 nm.

#### 3.1.5 X-Ray Diffraction (XRD) Study

The structure and crystallinity of the produced nanoparticles were evaluated by X-ray diffraction (XRD) crystallography. Iron oxide chemical makeup determines their color. XRD depicts the diffraction of X-rays by a crystal lattice. Peaks in the pattern correspond to constructive interference of X-rays scattered by crystal planes. The position and intensity of these peaks provide information about the crystal structure, including lattice spacing and orienta-

tion, helping identify crystalline phases in a sample. Due to the magnetite ( $\text{Fe}_3\text{O}_4$ ) structure, the color is jet-black. The jet-black color combines the magnetite ( $\text{Fe}_3\text{O}_4$ ) structure and  $\text{CH}_4\text{N}_2\text{O}$ , indicating the formation of an iron folate core-shell. A graphite crystal was used to monochromatize the incoming X-rays to a wavelength of 0.154 nm (Fig. 5).

### 3.1.6 Zeta Potential (ZP) Measurement

The stability of the particles was good as evidenced by the zeta potential, which existed in the  $-24 \pm 141.92$  mv range for iron oxide and  $-28.2 \pm 195.85$  mv for iron folate core-shell (Fig. 6). As the surface of the particles in a colloidal system is negatively charged, this lead to electrostatic repulsion between particles, preventing them from aggregating. In colloidal stability, a higher negative zeta potential is often associated with better dispersion and resistance to particle flocculation or coagulation.

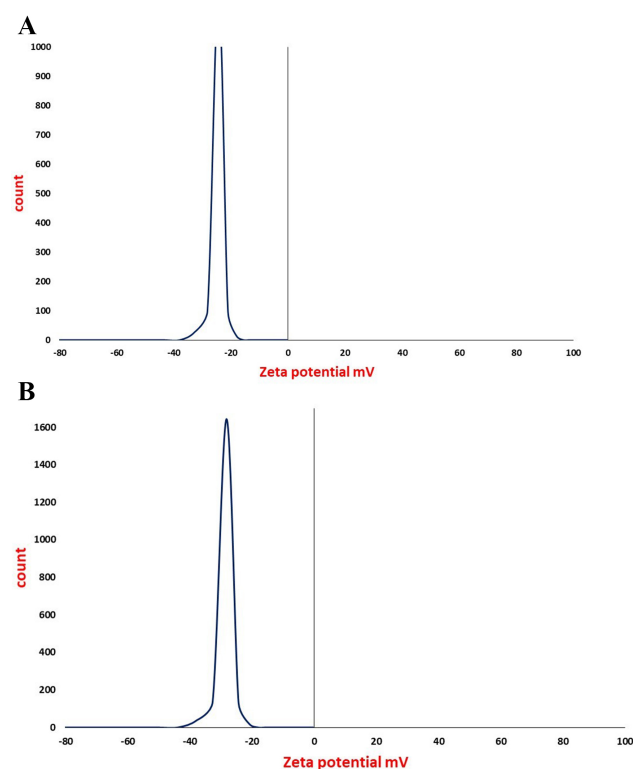


**Fig. 6.** Zeta potential analysis of (A) iron oxide and (B) iron folate core-shell nanoparticle which suggest that the surface of the particles in a colloidal system is negatively charged.

### 3.2 Cytotoxicity Analysis

In this study, the cells treated with various concentrations of iron oxide, iron folate core-shell nanocomposite, or doxorubicin were examined using the MTT test for the cytotoxicity of leukemia ALL (CCRF-CEM; RS4; 11) and AML (THP1; Kasumi-1), and normal (CRL-1980) cell lines (Table 2). The results showed that the presence of iron folate

core-shell nanocomposite reduced the viability of CCRF-CEM, RS4;11, and THP1 cells dose-dependently, while the cytotoxicity effect increased in Kasumi-1 and CRL-1980 cell lines (Fig. 7).

### 3.3 Analysis of Apoptotic and Necrotic Cells with Flow Cytometry

By analyzing Bax, Bcl2, and Caspase-3 activity in relation to different quantities of protein content for cells treated with the  $\text{IC}_{50}$  of iron oxide and iron folate core-shell NPs, the apoptotic impact of iron oxide and iron folate core-shell NPs was investigated (Table 3). Further research on the apoptotic impact of the iron oxide and iron folate core-shell NPs involved calculating the proportion of apoptotic cells using flow cytometric analysis and double-staining with Annexin V and propidium iodide. Meanwhile, Annexin V-negative/propidium iodide-negative staining denotes the presence of viable cells. In contrast, Annexin V-positive/propidium iodide-positive staining denotes the presence of cells that have undergone late apoptosis. Representative dot plots for the flow cytometric analysis comparing treated and untreated cells revealed that treated cells had higher percentages of early and late apoptosis than untreated cells.

### 3.4 Bax, Bcl-2, and Caspase-3 Subfamily Expression in Leukemia Cancer Lines

Our data demonstrate a high Bax and Caspase-3 expression level in the CCRF-CEM cell line treated with an iron folate core-shell compared with the THP cell line, while Bax and Caspase-3 expression in the CCRF-CEM and THP cell line treated with iron were slightly similar. On the other hand, Bcl-2 showed high expression in the THP cell line treated with iron compared with the CCRF-CEM cell line, while Bcl-2 expression in the CCRF-CEM and THP cell line treated with iron folate core-shell were slightly similar (Table 4, Fig. 8).

## 4. Discussion

UV-Vis spectroscopy was used to validate the production of nanoparticles. Fig. 1 displays the UV-Visible spectrum of iron oxide nanoparticles—iron oxide nanoparticles were present, as shown by the strong 250–300 nm peak. Bonvin *et al.* [22] and Niraimathee *et al.* [23] reported similar results. The created iron oxide nanoparticles were evenly distributed and nearly spherical, as seen in the TEM image in Fig. 2. The size range of the core-shell nanoparticles for iron oxide and iron folate was 7–42 nm. This finding is consistent with Guo *et al.* [24].

The FTIR examination of the synthetic iron oxide and iron folate core-shell nanoparticles yielded results in the 400–4000  $\text{cm}^{-1}$  wavenumber region, indicating the presence of both functional groups and chemical bonds (Fig. 3). Because  $\text{NH}_4\text{OH}$  was used to produce the  $\text{Fe}_2\text{O}_4$ -NPs, the absorption peaks at 1643  $\text{cm}^{-1}$  and 3441  $\text{cm}^{-1}$  indicated

**Table 2. The cytotoxicity analysis with different treatments.**

|        | Cell Lines          | IC <sub>50</sub> (µg/mL) |                        |               | p-value   |
|--------|---------------------|--------------------------|------------------------|---------------|---|
|        |                     | Iron                     | Iron folate core-shell | Doxorubicin   |   |
| ALL    | CCRF-CEM            | 46.8 ± 30.09             | 42.65 ± 31.1           | 14.8 ± 2.37   | $p_1 = 0.045^*$ ; $p_2 = 0.081$ ; $p_3 = 0.836$ |
|        | RS4;11              | 54.94 ± 35.8             | 48.2 ± 35.6            | 19.38 ± 8.0   | $p_1 = 0.062$ ; $p_2 = 0.115$ ; $p_3 = 0.773$   |
| AML    | THP1                | 60.29 ± 33.3             | 50.8 ± 29.34           | 24.24 ± 4.13  | $p_1 = 0.043^*$ ; $p_2 = 0.08$ ; $p_3 = 0.645$  |
|        | Kasumi-1            | 83.5 ± 8.4               | 85.83 ± 33.08          | 64.94 ± 19.02 | $p_1 = 0.081$ ; $p_2 = 0.256$ ; $p_3 = 0.883$   |
| Normal | COLO 829BL-CRL-1980 | 52.04 ± 32.89            | 70.54 ± 32.66          | 43.52 ± 20.33 | $p_1 = 0.636$ ; $p_2 = 0.155$ ; $p_3 = 0.398$   |

$p_1$ : p-value for comparing between iron- and doxorubicin (control)-treated cell lines;  $p_2$ : p-value for comparing between iron folate core-shell- and doxorubicin (control)-treated cell lines;  $p_3$ : p-value for comparing between iron- and iron folate core-shell-treated cell lines.

\*: Statistically significant at  $p \leq 0.05$ .

ALL, acute lymphocytic leukemia; AML, acute myelogenous leukemia.

**Table 3. Apoptosis and necrosis rates in early- and late-stage cells.**

|   |                             | Apoptosis   |  |   | Necrosis   |
|---|-----------------------------|---|--|---|--|
|   |                             | Total   | Early  | Late  |  |
| 1 | Iron/CCRF                   | 12.4 ± 0.16   | 5.1 ± 0.08   | 4.6 ± 0.8   | 2.7 ± 0.24   |
| 2 | Iron/THP                    | 10.2 ± 0.32   | 2.3 ± 0.16   | 5.8 ± 0.16  | 2.1 ± 0.48   |
| 3 | Iron folate core-shell/CCRF | 16.0 ± 0.4  | 5.3 ± 0.2  | 7.6 ± 0.2   | 3.1 ± 0.6  |
| 4 | Iron folate core-shell/THP  | 12.9 ± 0.24   | 4.3 ± 0.1  | 6.5 ± 0.2   | 2.1 ± 0.34   |
| 5 | cont. CCRF                  | 2.3 ± 0.41  | 1.4 ± 0.22   | 0.3 ± 0.22  | 0.6 ± 0.63   |
| 6 | cont. THP                   | 2.2 ± 0.25  | 1.3 ± 0.13   | 0.4 ± 0.15  | 0.5 ± 0.38   |
|   |                             | $p_1 = p < 0.0001^*$ ; $p_2 = p < 0.0001^*$ ; $p_3 = p < 0.0001^*$ ; $p_4 = p < 0.0001^*$ ; $p_5 = p < 0.0001^*$ ; $p_6 = p < 0.0001^*$ | $p_1 = p < 0.0001^*$ ; $p_2 = p < 0.0001^*$ ; $p_3 = p < 0.0001^*$ ; $p_4 = p < 0.0001^*$ ; $p_5 = 0.072$ ; $p_6 = p < 0.0001^*$ | $p_1 = p < 0.0001^*$ ; $p_2 = p < 0.0001^*$ ; $p_3 = p < 0.0001^*$ ; $p_4 = p < 0.0001^*$ ; $p_5 = p < 0.0001^*$ ; $p_6 = 0.0003^*$ | $p_1 = p < 0.0001^*$ ; $p_2 = p < 0.0001^*$ ; $p_3 = p < 0.0001^*$ ; $p_4 = p < 0.0001^*$ ; $p_5 = 0.204$ ; $p_6 = 1.0000$ |

$p_1$ : p-value for comparing between iron/CCRF and cont. CCRF;  $p_2$ : p-value for comparing between iron folate core-shell/CCRF and cont. CCRF;  $p_3$ : p-value for comparing between iron/THP and cont. THP;  $p_4$ : p-value for comparing between iron folate core-shell/and cont. THP;  $p_5$ : p-value for comparing between iron/CCRF and iron folate core-shell/CCRF;  $p_6$ : p-value for comparing between iron/THP and iron folate core-shell/THP.

\*: Statistically significant at  $p \leq 0.05$ .

**Table 4. Fold change in the expression of Bax, Bcl-2, and Caspase-3 using real-time PCR.**

| Treated Groups             | Bax        | Bcl-2                         | Caspase-3                     |
|----------------------------|------------|-------------------------------|-------------------------------|
| Iron/CCRF                  | 4.22 ± 0.4 | 0.26 ± 0.8                    | 3.54 ± 0.9                    |
| Iron/THP                   | 4.51 ± 0.6 | 0.33 ± 0.6                    | 3.76 ± 0.3                    |
| Iron folate coreshell/CCRF | 7.04 ± 0.4 | 0.19 ± 0.2                    | 4.35 ± 0.8                    |
| Iron folate coreshell/THP  | 4.61 ± 0.7 | 0.16 ± 0.7                    | 3.73 ± 0.7                    |
|                            |            | $p_1 = 0.854$ ; $p_2 = 0.691$ | $p_1 = 0.171$ ; $p_2 = 0.932$ |

$p_1$ : p-value for comparing between iron/CCRF and iron folate core-shell/CCRF;  $p_2$ : p-value for comparing between iron/THP and iron folate core-shell/THP.

\*: Statistically significant at  $p \leq 0.05$ .

the bending vibration of absorbed water and surface hydroxyl (–OH) groups [25]. The stretching vibration of the C–N group in aliphatic amine was responsible for the peak at 1095 cm<sup>-1</sup>. Due to the vibrational intrinsic stretching of the metal–oxygen bond vibrations (in this case, Fe–O), two distinct peaks appeared at 586 cm<sup>-1</sup> and 632 cm<sup>-1</sup>, indicating that the produced NPs were iron oxide [26,27]. A

prior study further supported these results, establishing that the produced nanoparticles were made of iron oxide [26]. Therefore, our findings using the FTIR study agreed with the characterization results reported by others.

The type of solvent used, as well as the duration of the chemical reaction, affected the particle size of the Fe<sub>3</sub>O<sub>4</sub> NPs. The size of the developed NPs was found to be in the

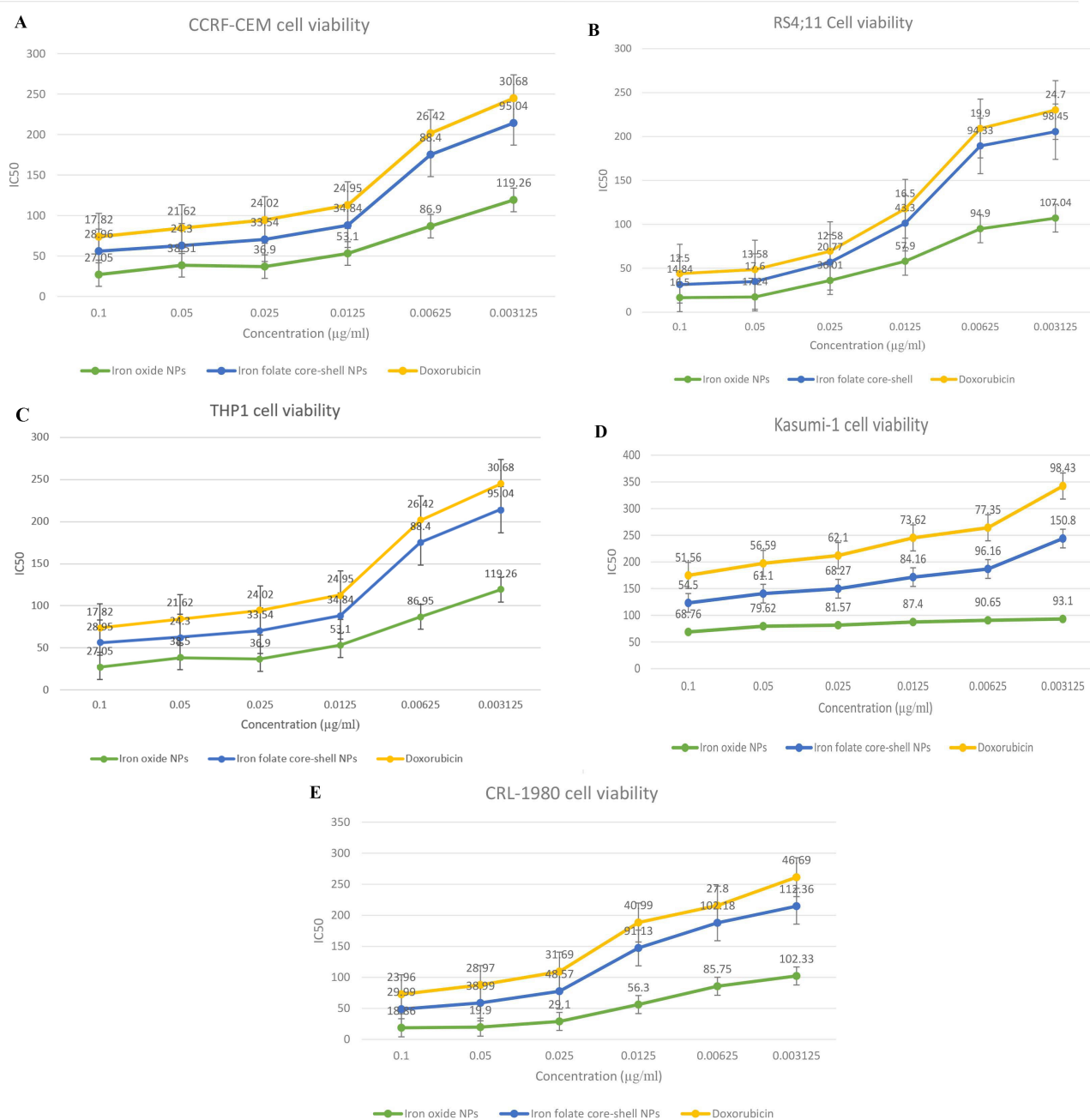


**Fig. 7. Cell viability in ALL, AML, and normal cell lines treated with ligands at various concentrations was determined using MTT assay to assess the anticancer activity of iron oxide, iron folate core-shell NPs, and doxorubicin on CCRF-CEM, RS4;11, THP1, Kasumi-1, and COLO 829BL-CRL-1980 cells.** Each cell line was subjected to a dose of a different treatment (0.003–0.1 µg/ml) for 24 h. Each data point shown is the mean ± SD from n = 3. The means of different groups differ significantly ( $p < 0.05$ ) by using a one-way analysis of variance. (A), (B), (C) and (E) showed lower IC50 values for iron folate core shell NPs with selected cell lines, which indicate a higher potency in inhibiting the growth of these cells by 50%. (D) showed a higher IC50 value for all selected NPs which indicate less potent of all selected NPs against Kasumi-1 cell line.

nanorange (1–100 nm) for metallic nanoparticles. Sizes for the iron oxide NPs in Fig. 4 were obtained using the DLS technique and were 33 nm and 55 nm, respectively. Compared to the sizes observed during TEM analysis, the average size of the NPs obtained using DLS was nearly identical and in agreement. The synthesized iron oxide and iron fo-

late core-shell's structure and crystallinity were evaluated using X-ray diffraction (XRD) crystallography (Fig. 5). A graphite crystal was used to monochromatize the incident X-rays to a wavelength of 0.154 nm. These findings agreed with the previous studies [25]. The color of iron oxides is a result of their chemical composition. The jet-black color

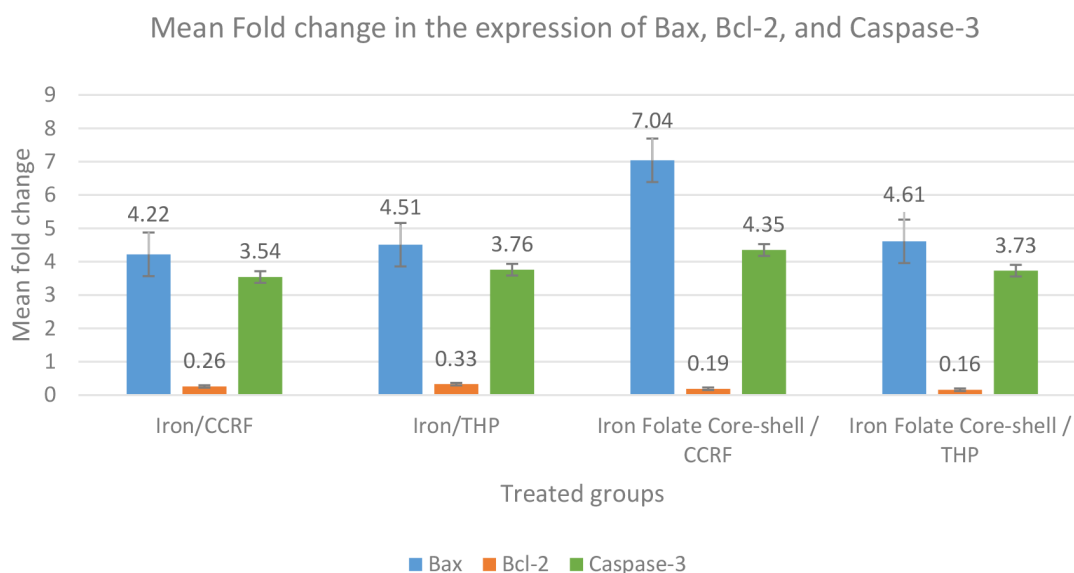


**Fig. 8. Expression changes of three apoptosis-associated proteins (Bax, Bcl-2, and Caspase-3) in the treated cells.** The data represented by the means of different groups differ significantly ( $p < 0.05$ ) by using a one-way analysis of variance.

refers to the magnetite ( $\text{Fe}_3\text{O}_4$ ) structure, and the iron folate core-shell was a mixture of the magnetite ( $\text{Fe}_3\text{O}_4$ ) structure and  $\text{CH}_4\text{N}_2\text{O}$ .

In general, zeta potential measurements of the iron oxide and iron folate core-shell nanoparticles revealed negative surface charges. Surface modification, however, could produce highly positively charged NPs for improved colloidal stabilization [28]. The zeta potential values were approximately  $-24 \pm 141.92$  mv for iron oxide NPs and approximately  $-28.2 \pm 195.85$  mv for iron folate core-shell, as shown in Fig. 6. This result agrees with Ostolska and Wiśniewska [29] and Răcuciu *et al.* [30], who reported that the ZP values of approximately -10 to -15 mV. On the other hand, Leonel *et al.* [31] reported that the zeta potential value was approximately -70 mV. Alangari *et al.* [32] produced iron oxide NPs with sufficiently high positive charges ( $\approx +20.8$  mV) on their surfaces, which may have been made possible by the use of  $\text{NH}_4\text{OH}$  during the synthesis of the NPs.

Various clinical results for identifying multiple efficacy-affecting components of nanomedicine are essential to address the intricacy surrounding disease progression, therapy, care, and recurrence risk. It is essential to balance effectiveness against the impact on healthy cells to minimize the adverse effects on the quality of life in this situation [32]. Various nanocarriers are described in the literature for their drug delivery systems to circumvent these restrictions in cancer treatment [33]. To assess the inhibitory effects of the free and conjugated nanoforms on cell growth in leukemia cell lines, we devised the conjugation between iron oxide and iron folate core-shell as a carrier in this study. Initially, the cell viability of leukemia ALL (CCRF-CEM; RS4; 11) and AML (THP1; Kasumi-1)

and normal (CRL-1980) cell lines were evaluated using the MTT method. The results showed the viability of CCRF-CEM; RS4; 11 and THP1 cells reduced dose-dependently in the presence of iron folate core-shell nanocomposite, while the cytotoxicity effect increased in Kasumi-1 and CRL-1980 cell lines (Fig. 7). The cytotoxicity effect of iron conjugated to folate core-shell was lower than iron oxide in a free nanoform. The  $\text{IC}_{50}$  values calculated for iron oxide NPs in cells were  $46.8 \pm 30.09$   $\mu\text{g}/\text{mL}$  (CCRF-CEM),  $54.94 \pm 35.8$   $\mu\text{g}/\text{mL}$  (RS4;11), and  $60.29 \pm 33.3$   $\mu\text{g}/\text{mL}$  (THP1) after treatment, while the  $\text{IC}_{50}$  values calculated for iron folate core-shell NPs were  $42.65 \pm 31.1$   $\mu\text{g}/\text{mL}$  (CCRF-CEM),  $48.2 \pm 35.6$   $\mu\text{g}/\text{mL}$  (RS4;11), and  $50.8 \pm 29.34$   $\mu\text{g}/\text{mL}$  (THP1) in treated cells. On the other hand, the cytotoxicity of iron showed that the  $\text{IC}_{50}$  values were  $83.5 \pm 8.4$   $\mu\text{g}/\text{mL}$  (Kasumi-1) and  $52.04 \pm 32.89$   $\mu\text{g}/\text{mL}$  (CRL-1980), which was lower than iron folate core-shell,  $85.83 \pm 33.08$   $\mu\text{g}/\text{mL}$  (Kasumi-1), and  $70.54 \pm 32.66$   $\mu\text{g}/\text{mL}$  (CRL-1980). The difference was not statistically significant ( $p = 0.993$ ).

The assessment of the number of apoptotic cells using flow cytometric analysis with the AV/PI double labeling provided additional evidence of the apoptotic impact of the induction of iron oxide and iron folate core-shell NPs. Phosphatidylserine is often translocated from the inner to the outer section of the plasma membrane to initiate an early apoptotic event. Green fluorescence is produced when annexin V binds to phosphatidylserines in the presence of calcium ions. These findings showed that late apoptosis or necrosis enhanced membrane permeability, allowing PI to enter cells. PI binds to cellular DNA and dyes the nucleus red. The findings showed that iron folate core-shell may cause apoptosis in CCRF-CEM and THP and that early apoptosis and necrosis could be observed in CCRF-

CEM treated with iron and iron folate core–shell, respectively. Results of our study revealed a rise in the percentage of annexin V-FITC and PI-positive cells (upper right quadrant) in a time-dependent manner, indicating late apoptosis (Table 3), with a significant difference between treatment groups with iron oxide NPs, iron folate core–shell NPs, and doxorubicin ( $p = 0.007$ ).

Currently, apoptosis is thought to be the primary cause of cell death. The antiapoptotic protein B-cell lymphoma-2 (Bcl-2) has an antiapoptotic function. The pro-apoptotic protein known as Bcl-2 associated X protein (Bax) can accelerate cell death. When Bcl-2 is overexpressed, it exerts an antiapoptotic impact because Bax has an antagonistic effect on the protein. Contrarily, when Bax is dominant, cells are more prone to apoptosis [34]. Both CRRF-CEM and THP cells were treated, which led to a reduction in Bcl-2 and an increase in *Bax* gene expression. This data indicated that nanoparticles predisposed these chemo-resistant malignant cells to induce apoptosis by altering gene expression. The most thoroughly researched effector, caspase, is caspase-3, which is activated in the perinuclear region of the cell and linked to the release of mitochondrial cytochrome c, which may be inhibited by upregulating Bcl-2 proteins [35]. Our investigation demonstrated that the combination of the folate core–shell and iron oxide NPs significantly increased the transcription and expression of caspase-3 in CCRF CEM cells. This finding confirms that IONPs enhance the folate core–shell-mediated apoptosis and this is linked to the gene and protein expression level. In cancerous cells, apoptosis can be initiated by activating molecules upstream of the signaling pathway or inhibiting antiapoptotic factors.

## 5. Conclusions

Our study shows that the combination of iron oxide and folate core–shell iron was an effective treatment for leukemia. Iron oxide and iron folate core–shell NPs were characterized by FTIR, XRD, TEM, and UV-Visible spectroscopy. The produced nanoparticles ranged in size from 7 to 42 nm, had appropriate monodispersity, and did not aggregate. With no toxicity and compatibility with normal cell lines, iron oxide and iron folate core–shell nanoparticles exhibited the right amount of cytotoxicity against acute leukemia malignancy. Therefore, synthetic iron oxide with a folate core–shell could be considered as a possible anti-cancer drug.

## Availability of Data and Materials

The data supporting the findings and conclusions are available and can be found in the article's manuscript; any additional data can be supplemented upon request.

## Author Contributions

GMN & MM designed the study. GMN, OMT & MM contributed to the practical work, study methodology, and

resources. GMN, MOE & RMT already feed the research by updated studies and review the writing and editing. All authors contributed to editorial changes in the manuscript. All authors read and approved the final manuscript. All authors have participated sufficiently in the work and agreed to be accountable for all aspects of the work.

## Ethics Approval and Consent to Participate

Not applicable.

## Acknowledgment

Not applicable.

## Funding

This research received no external funding.

## Conflict of Interest

The authors declare no conflict of interest.

## References

- [1] Jiang D, Wu X, Sun X, Tan W, Dai X, Xie Y, *et al.* Bone mesenchymal stem cell-derived exosomal microRNA-7-5p inhibits progression of acute myeloid leukemia by targeting OSBPL11. *Journal of Nanobiotechnology.* 2022; 20: 29.
- [2] Wu X, Li S, Chen D, Zheng G, Zhang Z, Li Z, *et al.* An inflammatory response-related gene signature associated with immune status and prognosis of acute myeloid leukemia. *American Journal of Translational Research.* 2022; 14: 4898–4917.
- [3] Wang Y, Yang Y, Zheng X, Shi J, Zhong L, Duan X, *et al.* Application of iron oxide nanoparticles in the diagnosis and treatment of leukemia. *Frontiers in Pharmacology.* 2023; 14: 1177068.
- [4] Locatelli F, Zugmaier G, von Stackelberg A. Blinatumomab vs Chemotherapy Among Children with Relapsed Acute Lymphoblastic Leukemia-Reply. *JAMA.* 2021; 326: 359–360.
- [5] Fu L, Ma X, Liu Y, Xu Z, Sun Z. Applying nanotechnology to boost cancer immunotherapy by promoting immunogenic cell death. *Chinese Chemical Letters.* 2022; 33: 1718–1728.
- [6] Peter S, Alven S, Maseko RB, Aderibigbe BA. Doxorubicin-Based Hybrid Compounds as Potential Anticancer Agents: A Review. *Molecules.* 2022; 27: 4478.
- [7] Chen H, Zheng D, Pan W, Li X, Lv B, Gu W, *et al.* Biomimetic Nanotheranostics Camouflaged with Cancer Cell Membranes Integrating Persistent Oxygen Supply and Homotypic Targeting for Hypoxic Tumor Elimination. *ACS Applied Materials & Interfaces.* 2021; 13: 19710–19725.
- [8] Zhao Y, Sun Y, Hang R, Yao R, Zhang Y, Huang D, *et al.* Biocompatible silane adhesion layer on titanium implants improves angiogenesis and osteogenesis. *Biomaterials Advances.* 2022; 139: 213033.
- [9] Abdoli M, Arkan E, Shekarbeygi Z, Khaledian S. Green synthesis of gold nanoparticles using *Centaurea behen* leaf aqueous extract and investigating their antioxidant and cytotoxic effects on acute leukemia cancer cell line (THP-1). *Inorganic Chemistry Communications.* 2021; 129: 108649.
- [10] Xu JJ, Zhang WC, Guo YW, Chen XY, Zhang YN. Metal nanoparticles as a promising technology in targeted cancer treatment. *Drug Delivery.* 2022; 29: 664–678.
- [11] Pillarsetti S, Uthaman S, Huh KM, Koh YS, Lee S, Park IK. Multimodal Composite Iron Oxide Nanoparticles for Biomedical Applications. *Tissue Engineering and Regenerative Medicine.* 2019; 16: 451–465.

- [12] Gonzalez-Rodriguez R, Campbell E, Naumov A. Multifunctional graphene oxide/iron oxide nanoparticles for magnetic targeted drug delivery dual magnetic resonance/fluorescence imaging and cancer sensing. *PLoS ONE*. 2019; 14: e0217072.
- [13] Cabana S, Curcio A, Michel A, Wilhelm C, Abou-Hassan A. Iron Oxide Mediated Photothermal Therapy in the Second Biological Window: A Comparative Study between Magnetite/Maghemite Nanospheres and Nanoflowers. *Nanomaterials*. 2020; 10: 1548.
- [14] Alphanđery E. Biodistribution and targeting properties of iron oxide nanoparticles for treatments of cancer and iron anemia disease. *Nanotoxicology*. 2019; 13: 573–596.
- [15] Carron PM, Crowley A, O’Shea D, McCann M, Howe O, Hunt M, *et al.* Targeting the Folate Receptor: Improving Efficacy in Inorganic Medicinal Chemistry. *Current Medicinal Chemistry*. 2018; 25: 2675–2708.
- [16] Zheng Y, Cantley LC. Toward a better understanding of folate metabolism in health and disease. *The Journal of Experimental Medicine*. 2019; 216: 253–266.
- [17] Deb A, Vimala R. Camptothecin loaded graphene oxide nanoparticle functionalized with polyethylene glycol and folic acid for anticancer drug delivery. *Journal of Drug Delivery Science and Technology*. 2018; 43: 333–342.
- [18] Mondal S, Adhikari A, Das M, Darbar S, Alharbi A, Ahmed SA, *et al.* Novel one pot synthesis and spectroscopic characterization of a folate-Mn<sub>3</sub>O<sub>4</sub> nanohybrid for potential photodynamic therapeutic application. *RSC Advances*. 2019; 9: 30216–30225.
- [19] Peng Y, Zhao Z, Liu T, Li X, Hu X, Wei X, *et al.* Smart Human-Serum-Albumin-As<sub>2</sub> O<sub>3</sub> Nanodrug with Self-Amplified Folate Receptor-Targeting Ability for Chronic Myeloid Leukemia Treatment. *Angewandte Chemie*. 2017; 56: 10845–10849.
- [20] Wu W, He Q, Chen H, Tang J, Nie L. Sonochemical synthesis, structure and magnetic properties of air-stable Fe<sub>3</sub>O<sub>4</sub>/Au nanoparticles. *Nanotechnology*. 2007; 18: 145609.
- [21] Devi HS, Boda MA, Shah MA, Parveen S, Wani AH. Green synthesis of iron oxide nanoparticles using *Platanus orientalis* leaf extract for antifungal activity. *Green Processing and Synthesis*. 2019; 8: 38–45.
- [22] Bonvin D, Arakcheeva A, Millán A, Piñol R, Hofmann H, Mionić E, *et al.* Controlling structural and magnetic properties of IONPs by aqueous synthesis for improved hyperthermia. *RSC Advances*. 2017; 7: 13159–13170.
- [23] Niraimathee VA, Subha V, Ramaswami S, Ernest R, Renganathan S. Green synthesis of iron oxide nanoparticles from *Mimosa pudica* root extract. *International Journal of Environment and Sustainable Development*. 2016; 15: 227.
- [24] Guo C, Weber RJM, Buckley A, Mazzolini J, Robertson S, Delgado-Saborit JM, *et al.* Environmentally Relevant Iron Oxide Nanoparticles Produce Limited Acute Pulmonary Effects in Rats at Realistic Exposure Levels. *International Journal of Molecular Sciences*. 2021; 22: 556.
- [25] Wang F, Qin XF, Meng YF, Guo ZL, Yang LX, Ming YF. Hydrothermal synthesis and characterization of  $\alpha$ -Fe<sub>2</sub>O<sub>3</sub> nanoparticles. *Materials Science in Semiconductor Processing*. 2013; 16: 802–806.
- [26] Hwang SW, Umar A, Dar G, Kim S, Badran R. Synthesis and characterization of iron oxide nanoparticles for phenyl hydrazine sensor applications. *Sensor Letters*. 2014; 12: 97–101.
- [27] Sharma P, Kumar R, Chauhan S, Singh D, Chauhan MS. Facile growth and characterization of  $\alpha$ -Fe<sub>2</sub>O<sub>3</sub> nanoparticles for photocatalytic degradation of methyl orange. *Journal of Nanoscience and Nanotechnology*. 2014; 14: 6153–6157.
- [28] Arakha M, Pal S, Samantarai D, Panigrahi TK, Mallick BC, Pramanik K, *et al.* Antimicrobial activity of iron oxide nanoparticle upon modulation of nanoparticle-bacteria interface. *Scientific Reports*. 2015; 5: 14813.
- [29] Ostolska I, Wiśniewska M. Application of the zeta potential measurements to explanation of colloidal Cr<sub>2</sub>O<sub>3</sub> stability mechanism in the presence of the ionic polyamino acids. *Colloid and Polymer Science*. 2014; 292: 2453–2464.
- [30] Răcuciu M, Barbu-Tudoran L, Oancea S, Drăghici O, Morosanu C, Grigoras M, *et al.* Aspartic Acid Stabilized Iron Oxide Nanoparticles for Biomedical Applications. *Nanomaterials*. 2022; 12: 1151.
- [31] Leonel AG, Mansur HS, Mansur AAP, Caires A, Carvalho SM, Krambrock K, *et al.* Synthesis and characterization of iron oxide nanoparticles/carboxymethyl cellulose core-shell nanohybrids for killing cancer cells *in vitro*. *International Journal of Biological Macromolecules*. 2019; 132: 677–691.
- [32] Alangari A, Mohammed AS, Ayesha M, Kalam MA, Alshemry A, Ali R, *et al.* Iron Oxide Nanoparticles: Preparation, Characterization, and Assessment of Antimicrobial and Anticancer Activity. *Adsorption Science & Technology*. 2022; 2022: 1562051.
- [33] Tousei MS, Sepehri H, Khoee S, Farimani MM, Delphi L, Mansourizadeh F. Evaluation of apoptotic effects of mPEG-b-PLGA coated iron oxide nanoparticles as a eupatorin carrier on DU-145 and LNCaP human prostate cancer cell lines. *Journal of Pharmaceutical Analysis*. 2021; 11: 108–121.
- [34] Yin X, Li Z, Lyu C, Wang Y, Ding S, Ma C, *et al.* Induced effect of zinc oxide nanoparticles on human acute myeloid leukemia cell apoptosis by regulating mitochondrial division. *IUBMB Life*. 2022; 74: 519–531.
- [35] Eskandari E, Eaves CJ. Paradoxical roles of caspase-3 in regulating cell survival, proliferation, and tumorigenesis. *The Journal of Cell Biology*. 2022; 221: e202201159.